MATERIALS AND INTERFACES

Effect of Zeolitization of CFBC Fly Ash on Immobilization of Cu^{2+}, Pb^{2+}, and Cr^{3+}

Feihu Li, Qin Li, Jianping Zhai,* and Guanghong Sheng

State Key Laboratory of Pollution Control and Resource Reuse, and School of the Environment, Nanjing University, Nanjing 210093, P. R. China

Two zeolitization processes, hydrothermal and molten-salt, were used to examine the effect of zeolitization of circulating fluidized-bed combustion (CFBC) fly ash on the immobilization of Cu^{2+}, Pb^{2+}, and Cr^{3+} in this study. As a consequence of zeolitization, most of the dissolved Cu^{2+}, Pb^{2+}, and Cr^{3+} had been immobilized in the synthetic aluminosilicate-aggregates-enriched matrixes under hydrothermal conditions, reaching maximum immobilization efficiencies of ∼89.1%, ∼82.4%, and ∼99.1%, respectively; whereas under molten-salt conditions, the synthetic cancrinite-enriched matrixes were most effective to immobilize Cu^{2+}, Pb^{2+}, and Cr^{3+} with maximum immobilization efficiencies of ∼94.5%, ∼50.7%, and ∼38.3%, respectively. Examinations of the synthetic matrixes by X-ray diffraction (XRD), scanning electron microscopy/energy-dispersive X-ray spectrometry (SEM/EDS), and sequential EDTA extractions suggest that physicochemical reactions responsible for the immobilization of heavy metal ions were ascribed to the speciation of insoluble species such as carbonates/silicates, hydroxides, and oxides and especially to the encapsulation of such species in aluminosilicates aggregates or cancrinite-enriched agglomerates. Furthermore, it is also proved that the speciation of soluble chromate in molten-salt processes contributed to the unexpected low immobilization efficiency of Cr^{3+} and that the Ca-enriched CFBC fly ash is an appropriate candidate for immobilization of Cu^{2+} and Pb^{2+}. Both zeolitization processes could be employed in solidification/stabilization of soils and sediments contaminated by heavy metals.

1. Introduction

As a promising and clean combustion technology, circulating fluidized-bed combustion (CFBC) is capable of burning a wide variety of fuels at a low temperature (800−950 °C) with high combustion efficiency and low NO_x emissions[1,2] and has been, therefore, widely operated by more and more power plants all over the world. When burning high-sulfur fuels such as petroleum coke, high-sulfur coal, and other sulfur-containing fuels, CFBC can efficiently desulfurize these fuels in situ by adding limestone simultaneously. The resultant CFBC fly ashes (CFAs) significantly vary from those of pulverized coal combustion[3] and possess considerable amounts of limestone and *f*-CaO due to the low calcium utilization efficiency (often <45%)[1] as well as high carbon content, especially in burning petroleum coke (PC) or PC−coal blends.[3−6] These factors led to the impracticability of utilizing CFBC fly ashes in the manufacture of construction materials such as cement and concrete area that consumes the great majority of pulverized coal combustion fly ashes (PFAs). Presently, the majority of these ashes are used for low-value structural infill and land reclamation purposes such as treating acidic waste in the strip-mined land or are sent for landfill disposal.[1,3] This study concerns the potential of employing CFA as starting materials for heavy metals immobilization by zeolitization in the presence of heavy metal ions.

Recently, many publications[7−10] have discussed the heavy metal immobilization technologies, most of which are based on the solidification/stabilization (S/S) principle employing complex mixtures of inorganic compounds (cement, lime, sodium silicates, clays, phosphates, coal fly ash, blast furnace slag, etc.) for the remediation of soils contaminated by heavy metals and/or the pretreatment of heavy-metal-containing industrial wastes (fly ashes from municipal solid waste incineration, mineral wastes, wastes from metallurgical industries, etc.) prior to landfill disposal and/or environment-friendly reuse.

As reviewed by Conner and Hoeffner,[7] these S/S technologies can be conveniently categorized as (i) chemical processes based on cement/fly ash mixture, pozzolan-based, lime/fly ash mixture, phosphate-based, miscellaneous bases, and additive intensive; (ii) physical process such as macroencapsulation and nonchemical microencapsulation; and (iii) thermal process such as thermoplastic polymer encapsulation and vitrification. In the case of heavy metal immobilization, chemical processes are generally involved in mechanisms including chemical-fixation of heavy metals into the neoformed matrix (geopolymer by geopolymetrization, C−S−H or C−A−H matrix by pozzolan-hydration, and agglomerate matrix by fusion, etc.); precipitation/coprecipitation of heavy metals as hydroxides, sulfides, carbonates, and other low-solubility forms; ion-exchange; oxidation/reduction of polyvalent heavy metal ions to a low-toxicity valence state, etc.[7,11] Physical processes commonly involve adsorbing or absorbing heavy metal ions on surfaces or in pores or encapsulating them in matrixes.

Zeolites, because of their chemical and structural characteristics, cation-exchange capacities, adsorption, and alkaline pH, have been widely used in contaminant immobilization.[12−14]

* Corresponding author. Phone/Fax: +86-25-8359 2903. E-mail: jpzhai@nju.edu.cn.

10.1021/ie070218v CCC: $37.00
Published on Web 09/22/2007

Table 1. Physiochemical Characteristics of CFBC Fly Ash

major oxides content (wt %)										
SiO_2	Al_2O_3	CaO	Fe_2O_3	Na_2O	MgO	K_2O	TiO_2	P_2O_5	SO_3	LOI[a]
40.20	24.70	15.21	2.94	0.35	0.52	0.46	1.16	0.12	0.17	12.45
trace elements content (mg/kg on dry basis)										
As	Cr	Cu	Cd	Se	Mo	Pb	Ni	V	U	Th
6.9	92.6	73	0.7	19.7	11.4	53.2	466.9	1233.5	9.3	19.7
leachable elements content by TCLP procedure (mg/L)										
Al^{3+}	Ba^{2+}	Ca^{2+}	Cr^{3+}	Cu^{2+}	Fe^{2+}	Pb^{2+}	Na^{+}	Si^{4+}	Zn^{2+}	Mg^{2+}
9.76	0.62	2348	0.32	1.60	1.32	N.A.	13.3	8.64	0.06	2.88
mineral components (wt %)										
quartz		calcite		anhydrite		albite		mullite		glass
8.42		7.67		4.17		0.66		0.34		78.74

[a] LOI = loss on ignition.

When using these materials for heavy metal immobilization, both chemical and physical process are involved. Cation exchange of metal ions with Na^+ or K^+ ions of zeolite, precipitating heavy metals as low-solubility hydroxides due to the increase of the solution pH by zeolite addition, and adsorbing or absorbing heavy metals on surfaces or in pores are mechanisms that take place. In addition, investigation on hydrothermal synthesis zeolite from fly ash and subsequent application in heavy metal immobilization has also been developed.[13−18] However, fly ashes used to synthesize zeolite were generally from pulverized coal combustion rather than CFBC, and the immobilization effect was estimated by addition of certain amount of synthetic zeolite to wastewater followed by evaluation of the retention of heavy metal ions. Terzano et al.[16] examined the effect of zeolite formation from fused coal fly ash in a Cu-polluted agricultural soil and demonstrated the immobilization potential of zeolite formation process from fly ash. Peña et al.[18] also proved that hydrothermal treatment of bottom ash from the incineration of municipal solid waste could efficiently immobilize heavy metal in the resultant zeolite-containing compound. Moreover, Choi et al.[19] presented a molten-salt method for zeolitization of fly ash, which may make it possible to evaluate the heavy metal immobilization potential of molten-salt zeolitization of CFBC fly ash as well.

The present study focuses on examining the effect of zeolitization of CFAs by both hydrothermal and molten-salt processes on the immobilization of Cu^{2+}, Pb^{2+}, and Cr^{3+} in the synthetic zeolite matrixes. X-ray diffraction (XRD) and scanning electron microscopy/energy-dispersive X-ray spectrometry (SEM/EDS) have been used to characterize the matrixes besides the evaluation of immobilization efficiency by EDTA sequential extractions with intention to disclose the immobilization mechanism.

2. Experimental Section

2.1. CFBC Fly Ash. The CFBC fly ash was obtained from a CFBC boiler of Jinling Power Plant (Nanjing, China), which cofired a fuel blend of bituminous coal and petroleum coke (50:50 cal %). The chemical and mineralogical characteristics are summarized in Table 1. The major oxide and trace element contents were determined by a ARL 9800 X-ray fluorescence spectrometer (XRF) with the fused- and pressed-disc methods, respectively.[6] The leaching test was determined according to toxic characteristic leaching procedure (TCLP) (EPA SW-846 Method 1311), and the leachate was measured by J-A1100 inductively coupled plasma quantometer (ICPQ, Jarrell-Ash). Mineralogical analysis was conducted using ARL X'TRA high-performance powder X-ray diffractometer (scanning step size, 0.02°; scanning rate, 5°/min; Cu Kα; 40 kV; 40 mA) at the Center of Modern Analysis (CMA), Nanjing University. Quantitative phase analysis of CFA was obtained by the reference intensity method (RIM), employing corundum as an internal standard.

Table 2. Experimental Conditions for Hydrothermal and Molten-Salt Processes

hydrothermal process	
sample	crystallization condition
H1	60 °C, 6 h
H2	60 °C, 12 h
H3	60 °C, 24 h
H4	90 °C, 6 h
H5	90 °C, 12 h
H6	90 °C, 24 h

molten-salt process			
sample	NaOH/CFA	$NaNO_3$/NaOH	crystallization condition
S1	0.2 (2 g:10 g)	0 (0 g:2 g)	250 °C, 12 h
S2	0.2 (2 g:10 g)	2 (4 g:2 g)	350 °C, 12 h
S3	0.2 (2 g:10 g)	5 (10 g:2 g)	450 °C, 12 h
S4	0.3 (3 g:10 g)	0 (0 g:3 g)	350 °C, 12 h
S5	0.3 (3 g:10 g)	2 (6 g:3 g)	450 °C, 12 h
S6	0.3 (3 g:10 g)	5 (15 g:3 g)	250 °C, 12 h
S7	0.5 (5 g:10 g)	0 (0 g:5 g)	450 °C, 12 h
S8	0.5 (5 g:10 g)	2 (10 g:5 g)	250 °C, 12 h
S9	0.5 (5 g:10 g)	5 (25 g:5 g)	350 °C, 12 h

2.2. Zeolite Synthesis and Characterization. Two zeolitization processes, hydrothermal and molten-salt, were followed to evaluate the effect of zeolitization of CFA on immobilization of heavy metal ions. Experimental conditions for both processes are listed in Table 2. As for the hydrothermal process, CFA has been previously activated using a fusion method[13] as follows: CFA was thoroughly mixed and ground with powdered NaOH (1:1, wt/wt) and then fused at 550 °C for 1 h in a muffle furnace and cooled to room temperature to obtain a sodium silicate-rich mixture.[13] After activation, 30 g of the mixture was ground and mixed with a blend of analytical-reagent-grade nitrates, 86 mg of $Cu(NO_3)_2{\cdot}3H_2O$, 36 mg of $Pb(NO_3)_2$, and 175 mg of $Cr_2(NO_3)_3{\cdot}9H_2O$, to obtain a final concentration of 1.5 (mg of $Cu^{2+}/Pb^{2+}/Cr^{3+}$)/(g of CFA). The mixture was dissolved in 300 mL of distilled water, followed by aging with stirring at 300 rpm for 4 h at 50 °C and subsequent curing with stirring at 300 rpm for 6, 12, and 24 h at 60 and 90 °C,

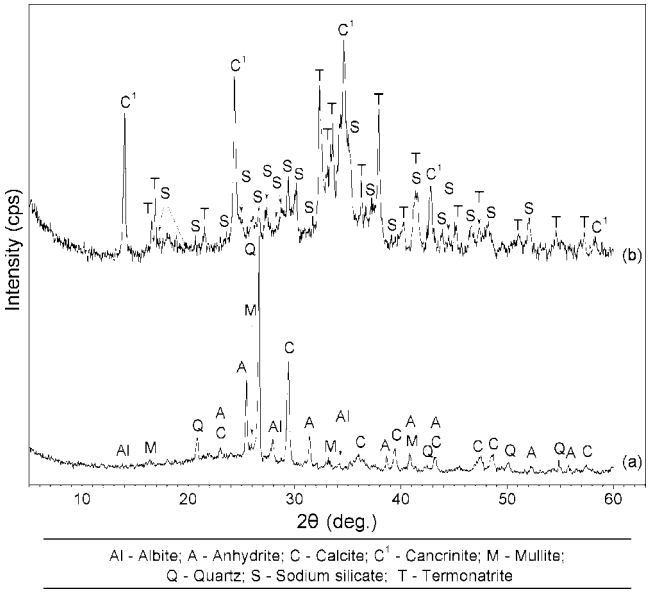

Figure 1. XRD patterns of CFA (a) and fused CFA (b).

respectively. At the end of each curing period, the solution was separated into a supernatant and a sediment by centrifugation. The supernatant was measured by ICPQ for Cu^{2+}, Pb^{2+}, and Cr^{3+} concentrations. The sediment (denoted as H1−H6) was dried at 80 °C for 12 h and kept for further tests.

The molten-salt process was performed with a NaOH/CFA ratio (wt/wt) of 0.2, 0.3, and 0.5 and a $NaNO_3$/NaOH ratio (wt/wt) of 0, 2, and 5, following the methodology indicated by Choi et al.[19] The mixture, consisting of CFA, NaOH, and $NaNO_3$, was combined with a blend of analytical-reagent-grade nitrates, 57 mg of $Cu(NO_3)_2{\cdot}3H_2O$, 24 mg of $Pb(NO_3)_2$, and 117 mg of $Cr_2(NO_3)_3{\cdot}9H_2O$ in order to ensure the final concentration in each sample being 1.5 (mg Cu^{2+}/Pb^{2+}/Cr^{3+})/(g of CFA). The resulting mixture was ground, then heated in a muffle furnace for 12 h at various temperatures (250, 350, and 450 °C), and finally cooled to room temperature and ground to yield the final matrixes (denoted as S1−S9).

Besides characterization of both synthetic matrixes by XRD with the above-mentioned parameters, scanning electron microscopy (SEM, JEOL JSM6300), coupled with energy-dispersive X-ray spectrometry (EDS, Oxford INCA 300) had also been performed at Nanjing Institute of Geology and Palaeontology (NIGP), CAS. Cation-exchange capacity (CEC) was also determined following U.S. EPA Method 9081 (sodium acetate) in addition to pH measurement with a slurry of 1 g of matrix and 10 mL of double-distilled water (shaken for 24 h at room temperature).

2.3. Heavy Metal Availability Test. A sequential EDTA extraction method was used to examine the availability of Cu^{2+}, Pb^{2+}, and Cr^{3+} immobilized in the synthetic matrixes. It was carried out as follows. A given amount of matrix (1.0 g for hydrothermal processes; 2% of the total amount of matrixes for molten-salt processes, assuming no loss occurred during the molten-salt processes) was added into a 50 mL Erlenmeyer flask, followed by addition of 30 mL of 0.01 M EDTA (sodium salt) solution and shaking for 12 h at room temperature. The suspension was centrifuged at 4000 rpm for 10 min, the supernatant was separated for heavy metal analysis by ICPQ, and the sediment was extracted with EDTA for a new cycle for 12 h. The sequential EDTA extraction was repeated 3 times. Figure 7 presents the results of sequential EDTA extractions.

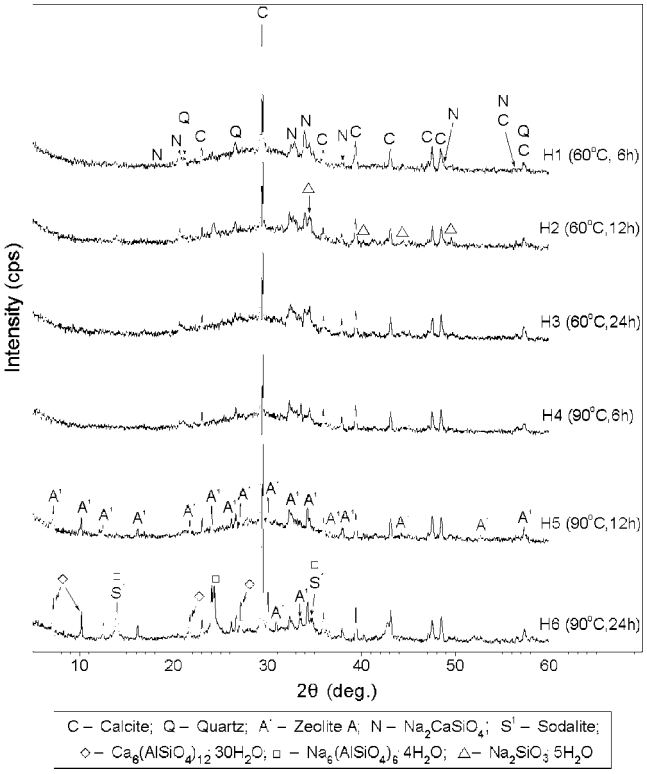

Figure 2. XRD patterns of matrixes synthesized by hydrothermal process (H1−H6).

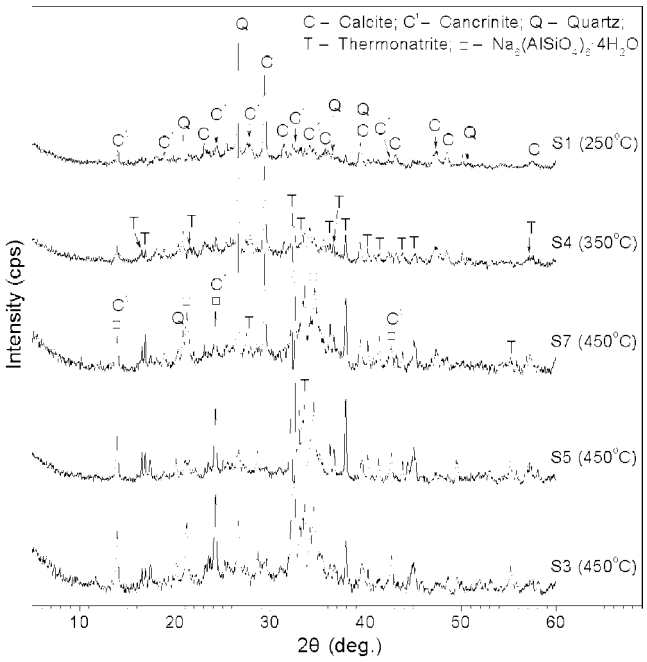

Figure 3. XRD patterns of matrixes synthesized by molten-salt process (S1, S3, S4, S5, and S7).

3. Results and Discussion

3.1. CFBC Fly Ash. The chemical analysis result shows that the CFA possesses a total amount of SiO_2 and Al_2O_3 of ~65% by weight, and the quantitative phase analysis result indicates that the CFA contains a high content of glass (78.74%, wt) with low contents of quartz (8.42%, wt) and mullite (0.34%, wt) (Table 1). It is, therefore, reasonable to conclude by mass balance that most of SiO_2 and Al_2O_3 are present in amorphous

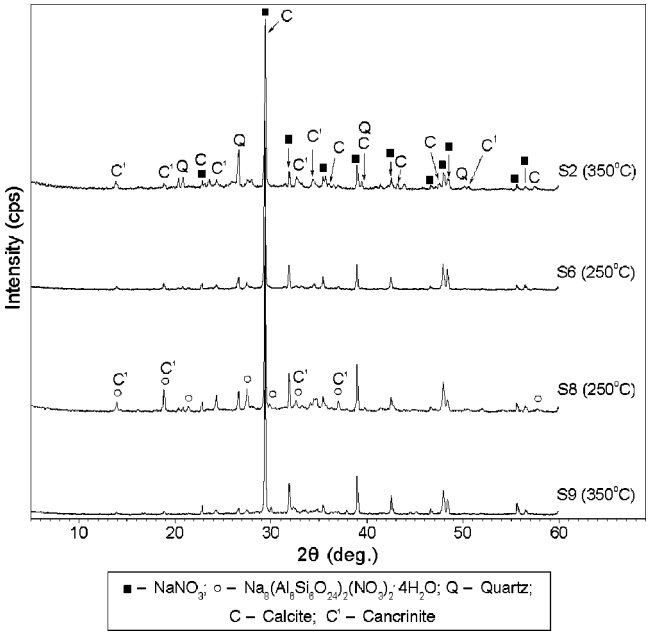

Figure 4. XRD patterns of matrixes synthesized by molten-salt process (S2, S6, S8, and S9).

species, which suggests that, with a hydrothermal treatment, CFA has a higher extraction potential of silicon and aluminum than the quartz- and mullite-rich PFA.[20]

Generally, CFA has a relatively high content of CaO derived from the excessive pulverized $CaCO_3$ injected in situ for SO_2 capture, which accounted for the formation of Ca-bearing species such as Na_2CaSiO_4, gismondine, and tobermorite in the zeolite matrixes.[21] As is concluded from the heavy metals content and leachate content (Table 1), Cu, Pb, and Cr in CFA cannot affect the final results of heavy metal immobilization.

Figure 1 compares the XRD patterns of CFA and fused CFA. The fused CFA shows an XRD pattern with strong peaks of cancrinite, sodium silicate, and thermonatrite, without any quartz peak, which further confirmed that the fusion process could effectively extract silicon from quartz and consequently form alkali-soluble siliceous species, which can be readily transformed to zeolite by hydrothermal treatment.[13]

3.2. Characterization of Zeolite Matrixes. Figure 2 shows the XRD patterns of zeolite matrixes by the hydrothermal process with variations of reaction time of 6, 12, and 24 h at 60 and 90 °C, respectively. As compared with the XRD pattern of the fused CFA, it is clearly noted that all the peaks of cancrinite, sodium silicate, and thermonatrite in the fused CFA disappeared after hydrothermal treatment. Instead, a strong calcite peak with several other phase peaks such as Na_2CaSiO_4 (marked with N), $Na_2SiO_3{\cdot}5H_2O$ (marked with □), zeolite A (marked with A^1), and sodalite (marked with S^1) appeared. The sharp increase of calcite peak intensity may result from the speciation of calcite by reaction of the high content of dissolved Ca^{2+} ions in the solution with CO_3^- from the dissolution of thermonatrite and CO_2 in the atmosphere.[22] The absence of zeolite phases in matrixes H1−H4 was probably due to the insufficiency of the reaction time.[15] As the reaction time increased to 12 and 24 h (H5, H6), zeolite A peaks appeared and a tiny increase in intensity of zeolite A peaks and a slight decrease in the amorphous halo between 15° and 35° in the 2θ range were distinctly observed. A few sodalite, $Na_6(AlSiO_4)_6{\cdot}4H_2O$ (marked with □), and $Ca_6(AlSiO_4)_{12}{\cdot}30H_2O$ (marked with ◇) peaks were also detected in H6. Besides, the speciation of zeolite A in matrixes H5 and H6 further confirms that the presence of heavy metal ions (Cu^{2+}, Pb^{2+}, and Cr^{3+}) in the solution does not hinder the formation of zeolite species.[16,17]

Figures 3 and 4 present the XRD patterns of zeolite matrixes synthesized by molten-salt process with variation of component ratios at 250, 350, and 450 °C. Comparing XRD patterns of S1, S4, and S7 in Figure 3, it can be clearly noted that, in the absence of $NaNO_3$, the major crystalline phases, quartz and calcite, remained after fusion at 250, 350, and 450 °C, respectively. Only a few small cancrinite peaks, thermonatrite peaks, and $Na_6(AlSiO_4)_6{\cdot}4H_2O$ peaks had been detected. Moreover, the intensities of cancrinite and thermonatrite peaks increase apparently with rising fusion temperature and increasing NaOH content (Table 2), implying higher fusion temperature and higher NaOH content favor the formation of both cancrinite and thermonatrite, despite the absence of $NaNO_3$ as solvent. With the addition of $NaNO_3$ to the starting materials, the intensity of the cancrinite peak increases apparently (S3 and S5), further demonstrating that introduction of $NaNO_3$ can greatly enhance the formation of cancrinite.[19] However, unlike the result reported in a previous study,[19] the introduction of $NaNO_3$ was not so effective to promote the formation of cancrinite (Figure 4) when the fusion temperature is <450 °C. This may possibly be because of the abundant calcite in CFA, but the credible reason for this observation should be further investigated.

Figures 5 and 6 present SEM microphotographs and EDS spectra of selected zeolite matrixes synthesized from CFA by hydrothermal and molten-salt processes, respectively. After hydrothermal treatment at 60 °C for 24 h (H3), only various aggregates (in a low-magnification SEM not shown herein) with some hexagonal crystal corresponding to Na_2CaSiO_4 according to the EDS spectrum (Figure 5b) were observed. Because the abundance of calcite detected by XRD could not be identified by SEM, it is therefore speculated that they were likely to be encapsulated by numerous aluminosilicate gels (zeolite precursors) and finally formed a great deal of aggregates as shown in Figure 5a. Under hydrothermal conditions for H5, many cubic crystals appeared (Figure 5c), which corresponds to zeolite A, in line with EDS analysis (Figure 5d), and is consistent with the results by XRD analysis. Besides cubic zeolite A, an abundance of needle and reticulated crystals appeared in H6, as shown in parts e and f of Figure 5. Analyses with EDS (Figure 5 parts f and h) indicate that the needle crystal relates to unnamed zeolite $Na_6(AlSiO_4)_6{\cdot}4H_2O$ and the reticulated crystal corresponds to $Ca_6(AlSiO_4)_{12}{\cdot}30H_2O$, both of which as well as zeolite A had been proved to have great immobilization capacity potential for heavy metals.[18,21] However, only irregular-shaped agglomerates and needle crystals without shaped crystals corresponding to cancrinite could be observed in S5 and S7 (Figure 6 parts a and c) because of the limitation of crystal growth in the molten-salt process and the embedding of such a crystal in amorphous agglomerates.[23] EDS analysis suggests that the agglomerate is rich in Na, Al, Si, and O (Figure 6b) and that the needle crystal rich in Na, O, and C probably corresponds to thermonatrite (Figure 6d).

The cation-exchange capacities (CECs) and alkalinities of CFA and matrixes synthesized by hydrothermal and molten-salt processes were presented in Table 3. After either hydrothermal or molten-salt treatments, the CECs of all matrixes increased apparently compared to that of the original CFA, and as expected, the hydrothermal matrixes exhibit higher CECs than the molten-salt matrixes. The CECs of hydrothermal matrixes with a ranking order of H2 > H1 = H3 > H4 > H5

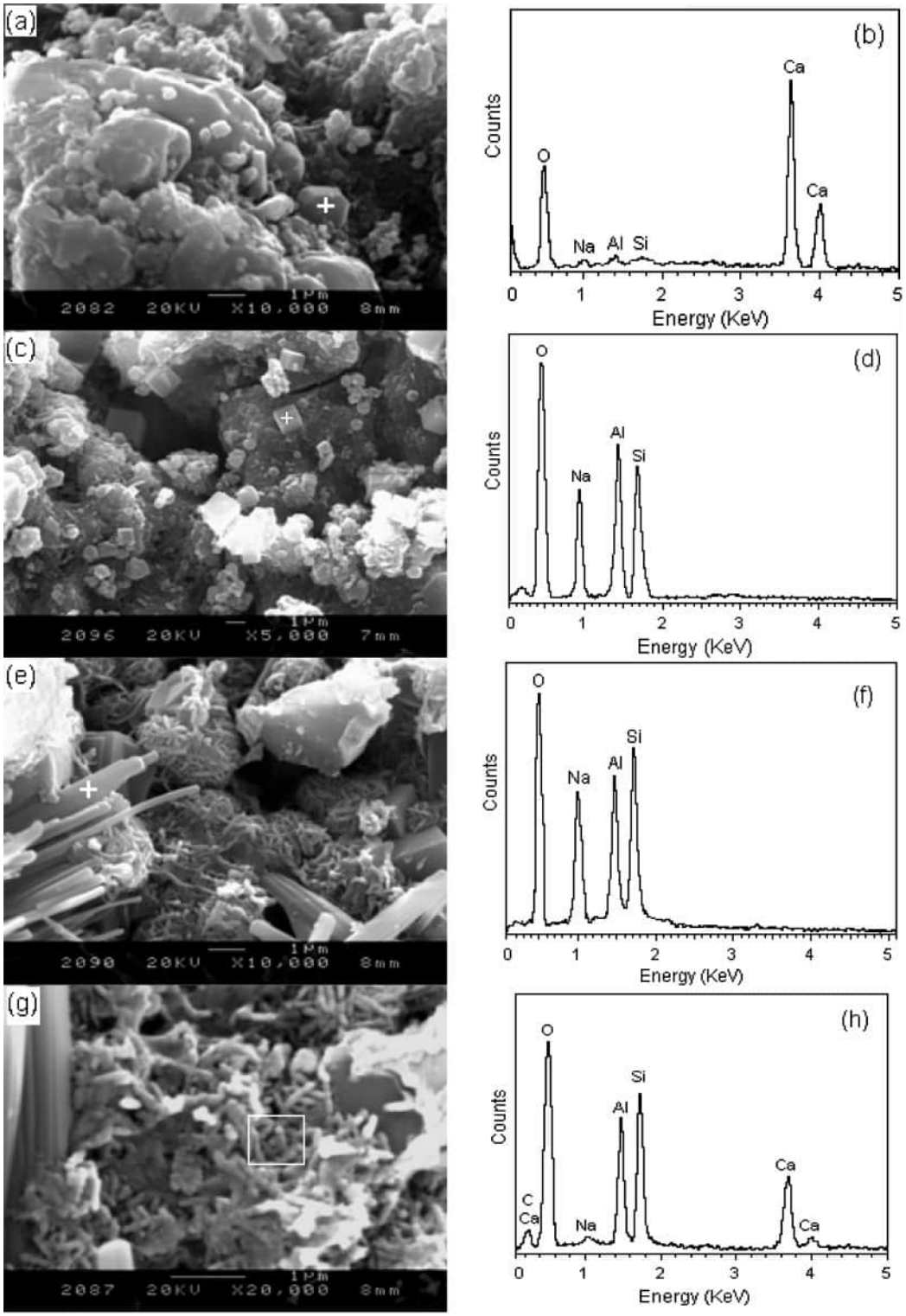

Figure 5. SEM micrographs and EDS spectra of selected matrixes synthesized by hydrothermal process: (a) H3; (b) EDS spectrum from spot marked with + in (a); (c) H5; (d) EDS spectrum from spot marked with + in (c); (e) H6; (f) EDS spectrum from spot marked with + in (e); (g) H6; and (h) EDS spectrum from area marked with □ in (g).

> H6 are somewhat in positive correlation with the variations of intensity of Na_2CaSiO_4 peaks but in reverse to the trend in intensity of zeolite A peaks (Figure 2), implying that the neoformed Na_2CaSiO_4 may contribute more than zeolite A to the CEC. On the other hand, the CECs of molten-salt matrixes are ranked in an order of S3 > S5 > S7 > S4 > S1 = S8 > S2 > S9 > S6, which is in agreement with the tendency in intensity of cancrinite peaks (Figures 3 and 4), suggesting the cancrinite in molten-salt matrixes should be responsible for their CECs. Moreover, all of the matrixes possess high alkalinity above or near 13 that is high enough to favor the precipitation of heavy metal ions.[10,17,18]

3.3. Heavy Metal Immobilization. Figure 7 shows the residual heavy metal ions (as (mg of $Cu^{2+}/Pb^{2+}/Cr^{3+}$)//(g of CFA) in the starting materials) in the solid phase after the EDTA sequential extractions. For matrixes from hydrothermal pro-

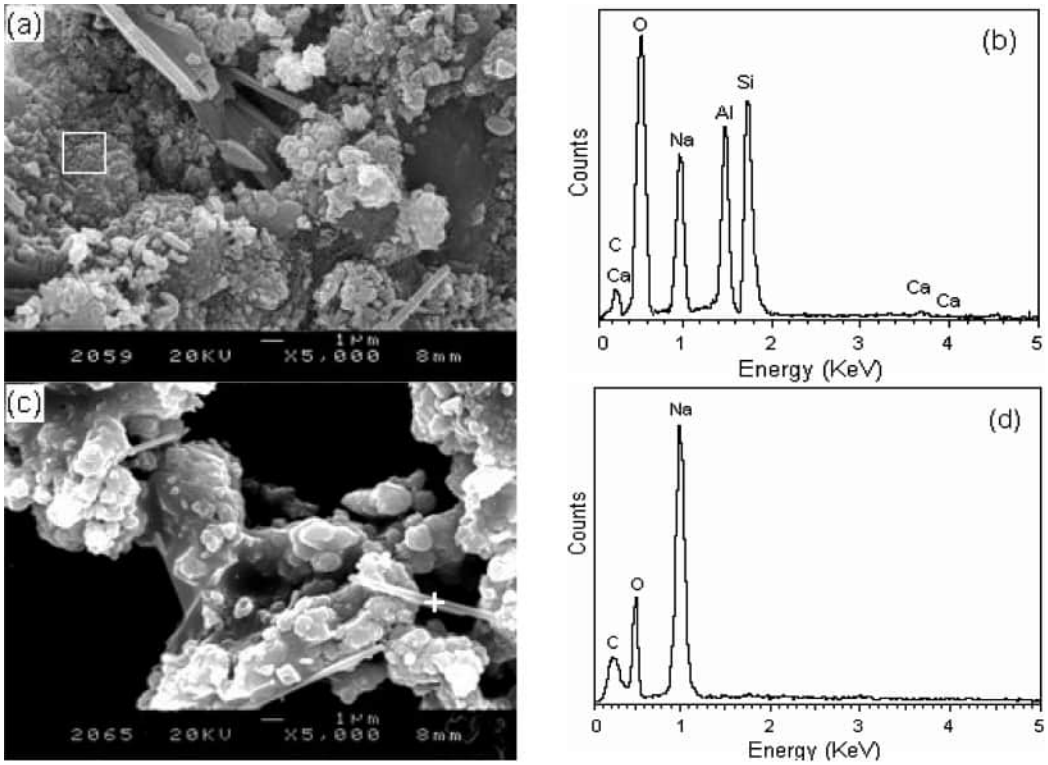

Figure 6. SEM micrographs and EDS spectra of selected matrixes synthesized by molten-salt process: (a) S5; (b) EDS spectrum from area marked with □ in (a); (c) S7; and (d) EDS spectrum from spot marked with + in (c).

cesses, the initial contents of heavy metal ions in the solid phase (C_S) were evaluated from the following equation: $C_S = C_0 - C_L$, where C_0 = the initial content of heavy metal ions in the starting materials (1.5 (mg of heavy metal ions)/(g of CFA)) and C_L = the final contents in the mother liquid phase, which varied for each individual condition, resulting in varying initial contents of residual heavy metal ions (C_S) as shown in Figure 7a. However, for matrixes from molten-salt processes, the initial contents of residual heavy metal ions (1.5 (mg of heavy metal ions)/(g of CFA)) can, assuming no mass loss occurred during the fusion process, be easily achieved by varying the amount of matrixes added to the same EDTA solution as illuminated in Section 2.3.

The matrix with the greatest Cu^{2+} immobilization efficiency of ~89.1% was, under hydrothermal conditions, H3, followed by H4 (i.e., ~88.3%) and H2 (i.e., ~86.5%), all of which were free of zeolite A while abundant in Na_2CaSiO_4 and other aluminosilicate aggregates, as indicated in Figures 2 and 5. However, H6 with the greatest amount of zeolite A (estimated by the intensity of zeolite A in Figure 2) among the hydrothermal matrixes had the least Cu^{2+} immobilization efficiency of ~7.2%. Moreover, because of the highly alkaline pH at all hydrothermal conditions (pH > 13), Cu was present in solution predominantly in anion−hydroxide forms, which implies that the cation-exchange reactions between Cu and the zeolite A could not take place and that cation exchange is not responsible for the immobilization of Cu^{2+}. Furthermore, hydrothermal treatment of the fused CFAs containing a large amount of thermonatrite would result in an abundance of carbonate ions (CO_3^{2-}) in the solution, which would lead to speciation of Cu−carbonate just like the speciation of calcite. Besides, Cu could be incorporated in the calcite structure during the formation of calcite according to Deja.[10] As concluded by the XRD analysis coupled with SEM observation above, calcite was encapsulated by the aluminosilicate gels to form a final geopolymer-like aggregate in the case of no zeolite formation (H2−H4); consequently, Cu−carbonate together with the resultant Cu-$(OH)_2$ and/or CuO were presumably embedded in the aluminosilicate aggregate as well, leading to immobilization of Cu.

On the other hand, when prolonging the hydrothermal reaction time (H5, H6), the outside aluminosilicate gels would redissolve to give rise to zeolite, which led to disassembly of the aggregates, resulting in exposure of the Cu−carbonates precipitates. As a consequence, more Cu^{2+} will be extracted by EDTA compared to the case of no zeolite formation (H2−H4), which is in great agreement with the results of sequential EDTA extractions (Figure 7a). Assuming that the hydrothermal reaction time was prolonged up to 1 year, in the case of no zeolite formation, the aluminosilicate aggregates should be gradually converted to zeolites, which were likely to further incorporate Cu-bearing compounds in their structures, as observed by Terzano et al.[16]

As for Pb^{2+} immobilization under hydrothermal conditions, similar results as for Cu^{2+} immobilization were observed, i.e., the zeolite-free matrix H2 immobilized most of Pb^{2+} in the solid phase (i.e., ~82.4%), followed by H4 (i.e., ~81.9%) and H3 (i.e., ~80.7%), whereas the zeolite-containing matrix H6 immobilized the least amount of Pb^{2+} (i.e., ~71.4%). This further confirms the active role of the aluminosilicate aggregates in immobilization of heavy metal ions mainly by encapsulation and suggests that Pb^{2+} follows the same immobilization mechanisms as Cu^{2+}. Unlike the case of Cu^{2+} and Pb^{2+}, besides Cr−carbonate, Cr was likely to present as insoluble Cr_2O_3 rather than as both $Cr(OH)_3$ and Cr_2O_3 because of the decomposition of $Cr(OH)_3$ during the drying process at 80 °C, which seems to be responsible for the relatively high immobilization efficiency of exceeding 98% (max. ~99.1% assigned to H4) for all hydrothermal conditions studied. Therefore, it could be concluded that, for hydrothermal processes, it is the speciation of carbonates as well as hydroxides and oxides and especially the following encapsulation of such compounds by geopolymer-

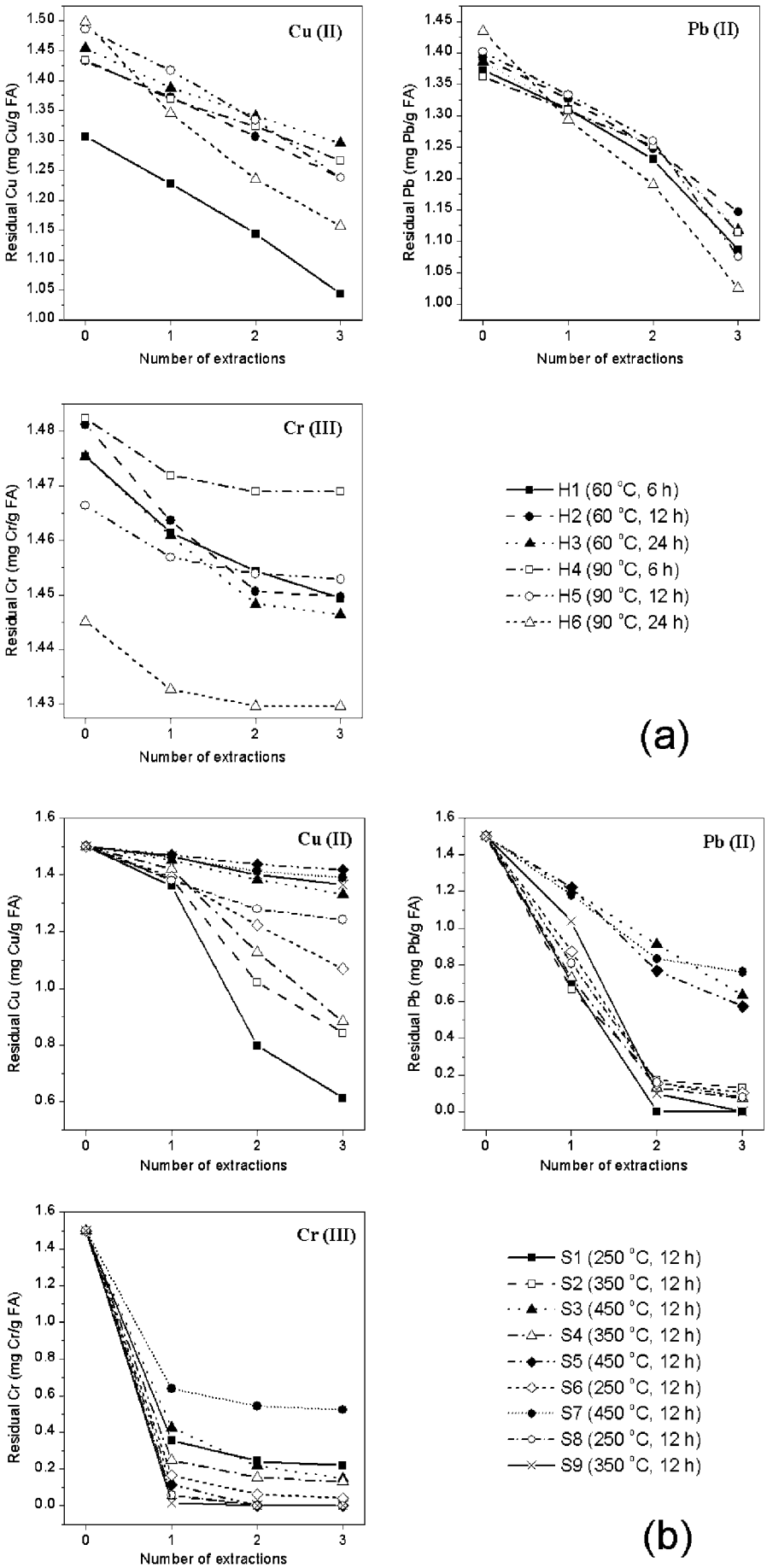

Figure 7. Residual heavy metal ions in the solid phase following EDTA extraction as a function of the number of extractions: (a) matrixes by hydrothermal process and (b) matrixes by molten-salt process.

Table 3. CEC and Alkalinity of CFA and Matrixes Synthesized by Hydrothermal and Molten-Salt Processes

sample	CFA	H1	H2	H3	H4	H5	H6	S1
CEC (mequiv/g)	0.12	1.74	1.88	1.74	1.69	1.63	1.41	0.6
pH	12.37	13.51	13.58	13.58	13.66	13.61	13.63	12.97
sample	S2	S3	S4	S5	S6	S7	S8	S9
CEC (mequiv/g)	0.56	1.07	0.71	0.99	0.49	0.72	0.6	0.53
pH	12.55	13.44	13.42	13.66	12.82	13.58	13.29	12.91

like aluminosilicate aggregates rather than cation exchanges that are responsible for immobilizations of the heavy metal ions.

Under molten-salt conditions, the matrix that immobilized most of Cu^{2+} was S5 (i.e., ~94.5%), followed by S7 (i.e., ~92.6%), both of which were synthesized at 450 °C and abundant in cancrinite, as illuminated in Figure 3, whereas S1 synthesized at 250 °C had the least immobilization efficiency (~40.8%). As reported by Jakob et al.,[24] the Cu may react with silica to form Cu−silicate under fusion of fly ash from a municipal solid waste incinerator (MSWI) in the temperature range of 670−1000 °C. Moreover, Sung et al.[25] also proved that, by fusion of MSWI fly ash with added silica and alumina in the temperature range of 700−900 °C, heavy metals including Cu^{2+} and Pb^{2+} can be immobilized in the resultant calcium aluminates or calcium aluminosilicates. Also, as reported in previous works,[13,19] fusion of fly ash with NaOH at 450 °C would result in decomposition of quartz (also proved by XRD as shown in Figure 1) and then formation of cancrinite and aluminosilicate agglomerates. It is, therefore, reasonable to conclude that the immobilization of Cu^{2+} was obtained, under fusion at 450 °C, by both the speciation of inert Cu-bearing compounds such as CuO, $Cu(OH)_2$, and Cu−silicate by incorporation of CuO in forming silicates, and the encapsulation of such compounds in neoformed cancrinite, $Na_6(AlSiO_4)_6 \cdot 4H_2O$, and other aluminosilicate agglomerates (Figure 6), which were limited to form at 250 °C.

Analogous to Cu^{2+}, speciation of Pb−silicate could also occur by the reaction of PbO with silicates.[24] Furthermore, similar results were observed for Pb^{2+} immobilization as shown in Figure 7b, suggesting that Pb^{2+} followed the mechanism for immobilization of Cu^{2+} as well. In addition, the immobilization efficiency of Pb^{2+} was less than that of Cu^{2+} for each matrix (i.e., for Pb^{2+}, max. ~50.7% assigned to S7); this was because of the fact that the solubility of PbO is greater than those of CuO and $Cu(OH)_2$ under the same conditions.

In the case of Cr^{3+}, however, the immobilization efficiency was unexpectedly <15% for almost all matrixes synthesized by molten-salt processes, with the exception of S7 (i.e., ~38.3%) synthesized at 450 °C. According to a previous investigation,[26] Cr^{3+} in MWSI fly ash could be, when fused under atmosphere conditions, oxidized to form soluble chromates, especially calcium chromate in a calcium-rich system. This seems suitable to explain the unexpected behavior of Cr^{3+} in our experiments. Experimental evidence could also be found by comparing the immobilization efficiencies and XRD patterns (Figure 3) of S3, S5, and S7 (all synthesized at 450 °C). The disappearance of calcite peaks and the enhancement of Cr^{3+} solubility in S3 and S5 compared to those of S7 indicated the formation of calcium chromate indeed occurred in the $NaOH-NaNO_3$ system. As for S7 without $NaNO_3$ added as solvent, the calcite remained and soluble chromate seems to be excluded in the final matrix, and likewise, the encapsulation of Cr-bearing compounds in cancrinite and other aluminosilicate agglomerates still contributed primarily to the immobilization of Cr^{3+} in the final product.

In addition, because of the limitation of diffusion for the heavy metal ions in molten-salt processes, cation-exchange reactions between the heavy metal ions and cancrinite did not occur and, consequently, cation exchange was not responsible for the immobilizations of such heavy metal ions. Analogous to hydrothermal conditions, immobilization of heavy metal ions for molten-salt processes should be owing to the speciation of silicates as well as hydroxides and oxides and especially the encapsulation of such resultant compounds by cancrinite and aluminosilicate agglomerates derived from the fusion process.

4. Conclusions

Under hydrothermal conditions of treating at 60 and 90 °C, zeolitization of CFBC fly ash in the presence of Cu^{2+}, Pb^{2+}, and Cr^{3+} could play an active role in immobilization of the heavy metal ions in the solid phase. The maximum immobilization efficiencies of Cu^{2+}, Pb^{2+}, and Cr^{3+} in the solid phase were attributed to the aluminosilicate-aggregates-enriched matrixes and were ~89.1%, ~82.4%, and ~99.1%, respectively. The mechanism accounting for immobilization of the heavy metal ions was ascribed primarily to the speciation of carbonates as well as hydroxides and oxides and especially to the encapsulation of such resultant compounds in geopolymer-like aluminosilicate aggregates, which tend to be converted into zeolites upon long-term hydrothermal treatments and further incorporate heavy metal ions in their structures, as observed by Terzano et al.[16] Likewise, zeolitization of CFA by molten-salt processes, especially those of fusion at 450 °C (S3, S5, and S7), could also effectively immobilize Cu^{2+} and Pb^{2+} in the final cancrinite-enriched matrixes, and the immobilization mechanism involves the speciation of silicates, hydroxides, and/or oxides and the encapsulation of such species in the cancrinite and other aluminosilicate agglomerates. However, with thermal treatment with $NaNO_3$ addition, the immobilization efficiency of Cr^{3+} was unexpectedly low, which was because of both the high content of $CaCO_3$ in CFA and the introduction of $NaNO_3$ promoting the reaction between synthetic Cr_2O_3 and CaO to produce soluble $CaCrO_4$, as reported by Kirk and co-workers.[26]

Nevertheless, the effective performances of both zeolitization processes in immobilization of heavy metal ions will allow us to employ them in solidification/stabilization of heavy-metal-contaminated soils, sediments, and especially MSWI fly ash. Moreover, it is proved that the Ca-enriched CFBC fly ash is an appropriate candidate for solidification/stabilization of heavy metal ions with the exception of immobilization of Cr^{3+} by the molten-salt process.

Acknowledgment

The authors are indebted to Jiyuan Brother Materials Co., Ltd., for supplying corundum and to Jinling Power Plant for providing CFBC fly ash. We also thank Dr. H. Yu of CMA for his XRD work, Mr. Y. Mao of NIGP for his detailed SEM/EDS analysis, and Mr. C. Chen for his CEC experimental assistance. The two anonymous reviewers are greatly appreciated for their valuable comments and suggestions on earlier versions of the manuscript.

Literature Cited

(1) Anthony, E. J. Fluidized bed combustion of alternative solid fuels; Status, successes and problems of the technology. *Prog. Energy Combust. Sci.* **1995**, *21*, 239−268.

(2) Nowak, W. Clean coal fluidized-bed technology in Poland. *Appl. Energy* **2003**, *74*, 405−413.

(3) Hall, M. L.; Livingston, W. R. Fly ash quality, past, present and future, and the effect of ash on the development of novel products. *J. Chem. Technol. Biotechnol.* **2002**, *77*, 234−239.

(4) Bryers, R. W. Utilization of petroleum coke and petroleum coke/coal blends as a means of steam raising. *Fuel Process. Technol.* **1995**, *44*, 121−141.

(5) Hower, J. C.; Robertson, J. D.; Roberts, J. M. Petrology and minor element chemistry of combustion by-products from the co-combustion of coal, tire-derived fuel, and petroleum coke at a western Kentucky cyclone-fired unit. *Fuel Process. Technol.* **2001**, *74*, 125−142.

(6) Li, F. H.; Zhai, J. P.; Fu, X. R.; Sheng, G. H. Characterization of fly ashes from circulating fluidized bed combustion (CFBC) boilers cofiring coal and petroleum coke. *Energy Fuels* **2006**, *20*, 1411−1417.

(7) Conner, J. R.; Hoeffner, S. L. A critical review of stabilization/solidification technology. *Crit. Rev. Environ. Sci. Technol.* **1998**, *28*, 397−462.

(8) Ahmed, Y. H.; Buenfeld, N. R. An investigation of ground granulated blastfurnace slag as a toxic waste solidification/stabilization reagent. *Environ. Eng. Sci.* **1997**, *14*, 113−132.

(9) Kilinckale, F.; Ayhan, S.; Apak, R. Solidification/stabilization of heavy metal-loaded red muds and fly ashes. *J. Chem. Technol. Biotechnol.* **1997**, *69*, 240−246.

(10) Deja, J. Immobilization of Cr^{6+}, Cd^{2+}, Zn^{2+} and Pb^{2+} in alkali-activated slag binders. *Cem. Concr. Res.* **2002**, *32*, 1971−1979.

(11) Spagnuolo, M.; Martínez, C. E.; Jacobsona, A. R.; Baveye, P.; McBridea, M. B. Newtond, J. Coprecipitation of trace metal ions during the synthesis of hectorite. *Appl. Clay Sci.* **2004**, *27*, 129−140.

(12) Lin, C.-F.; Lo, S.-S.; Lin, H.-Y.; Lee, Y. Stabilization of cadmium contaminated soils using synthesized zeolite. *J. Hazard. Mater.* **1998**, *60*, 217−226.

(13) Chang, H. L.; Shih, W. H. A general method for the conversion of fly ash into zeolites as ion exchangers for cesium. *Ind. Eng. Chem. Res.* **1998**, *37*, 71−78.

(14) Chang, H. L.; Shih, W. H. Synthesis of zeolites A and X from fly ashes and their ion-exchange behavior with cobalt ions. *Ind. Eng. Chem. Res.* **2000**, *39*, 4185−4191.

(15) Querol, X.; Moreno, N.; Umana, J. C.; Alastuey, A.; Hernandez, E.; Lopez-Soler, A.; Plana, F. Synthesis of zeolites from coal fly ash: an overview. *Int. J. Coal Geol.* **2002**, *50*, 413−423.

(16) Terzano, R.; Spagnuolo, M.; Medici, L.; Vekemans, B.; Vincze, L.; Janssens, K.; Ruggiero, P. Copper stabilization by zeolite synthesis in polluted soils treated with coal fly ash. *Environ. Sci. Technol.* **2005**, *39*, 6280−6287.

(17) Querol, X.; Alastuey, A.; Moreno, N.; Alvarez-Ayuso, E.; García-Sánchez, A.; Cama, J.; Ayora, C.; Simón, M. Immobilization of heavy metals in polluted soils by the addition of zeolite material synthesized from coal fly ash. *Chemosphere* **2006**, *62*, 171−180.

(18) Peña, R.; Guerrero, A.; Goñi, S. Hydrothermal treatment of bottom ash from the incineration of municipal solid waste: Retention of Cs(I), Cd(II), Pb(II) and Cr(III). *J. Hazard. Mater.* **2006**, *129*, 151−157.

(19) Choi, C. L.; Park, M.; Lee, D. H.; Kim, J. E.; Park, B. Y.; Choi, J. Salt-thermal zeolitization of fly ash. *Environ. Sci. Technol.* **2001**, *35*, 2812−2816.

(20) Moreno, N.; Querol, X.; Plana, F.; Andres, J. M.; Janssen, M.; Nugteren, H. Pure zeolite synthesis from silica extracted from coal fly ash. *J. Chem. Technol. Biotechnol.* **2002**, *77*, 274−279.

(21) Moutsatsou, A.; Stamatakis, E.; Hatzitzotzia, K.; Protonotarios, V. The utilization of Ca-rich and Ca−Si-rich fly ashes in zeolites production. *Fuel* **2006**, *85*, 657−663.

(22) Inada, M.; Eguchi, Y.; Enomoto, N.; Hojo, J. Synthesis of zeolite from coal fly ashes with different silica−alumina composition. *Fuel* **2005**, *84*, 299−304.

(23) Park, M.; Choi, C. L.; Lim, W. T.; Kim, M. C.; Choi, J.; Heo, N. H. Molten-salt method for the synthesis of zeolite materials II. Characterization of zeolite materials. *Microporous Mesoporous Mater.* **2000**, *37*, 91−98.

(24) Jakob, A.; Stucki, S.; Struis, R. P. W. J. Complete heavy metal removal from fly ash by heat treatment: influence of chlorides on evaporation rates. *Environ. Sci. Technol.* **1996**, *30*, 3275−3283.

(25) Sung, H. J.; Kamiya, K.; Noda, R.; Horio, M. Mineralogical stabilization of heavy metals from alkali melting furnace fly ash by thermal treatment with adjustment of its chemical composition. *J. Chem. Eng. Jpn.* **2005**, *38*, 1054−1068.

(26) Kirk, D. W.; Chan, C. C. Y.; Marsh, H. Chromium behavior during thermal treatment of MSW fly ash. *J. Hazard. Mater.* **2002**, *90*, 39−49.

Received for review February 7, 2007
Revised manuscript received June 22, 2007
Accepted August 2, 2007

IE070218V